2020 IEEE/RSJ International Conference on Intelligent Robots and Systems (IROS)
October 25-29, 2020, Las Vegas, NV, USA (Virtual)

Experimental Verification of Vibratory Conveyor System Based on Frequency Entrainment of Limit Cycle Walker*

Kento Mitsuhashi, Masatsugu Nishihara and Fumihiko Asano

***Abstract*— The authors have investigated underactuated locomotion robots with an inner wobbling mass, it is discovered that the wobbling mass controls the gait speed by entrainment. Supplying the wobbling from outside, outer wobbling entrains load objects and controls the transferring speed. In this paper, we propose a vibratory conveyor system based on the frequency entrainment of a limit cycle walker. The conveyance plate is vibrated by an active rimless wheel, and the system conveys a passive rimless wheel which is defined as a load object. The vibration entrains transferring of the passive rimless and controls the conveyance speed. First, we introduce the prototype experimental system and its mathematical model. Second, we report basic behavior of the passive rimless with regards to the outer vibration and results of frequency analysis through the numerical simulation. Third, we experimentally verify the results of the numerical simulation. The active rimless wheel entrains the walking frequency of the passive rimless wheel in both the simulations and the experiments.**

I. INTRODUCTION

Reducing complexity of the mechanism as well as the energy consumption are essential problems for industrial systems. Full actuation systems are suitable for stabilization of the motion, however the energy consumption increases with DoF of the system. To diminish the number of actuators, underactuated systems have been investigated as a solution of the essential problems [1][2]. The authors have also investigated underactuated sliding robots utilizing inner wobbling, the inner wobbling generates a body rotation and steady forward motion [3][4]. On a bipedal compass walker, inner wobbling added yawing motion control [5]. On limit cycle walking, wobbling an inner mass generates the steady gait at level surface [6] and entrains the walking frequency [7][8].

Based on these knowledge, we propose a vibratory conveyor system shown in Fig. 1. Supplying a vibration from outside, the vibration entrains load objects and controls the transferring speed. The conveyance plate is linearly vibrated by an active rimless wheel (ARW) shown under the conveyance plate. A vibratory conveyor system conveys small objects in one dimension [9] or two dimensions [10], they considers only transferring the objects. A manipulation system achieves three-DoF planar motions by a single actuator, the system manipulates the position and the orientation of the object [11]. Although these systems control the position or the orientation on the horizontal plane with respect to the plate, a motion on the vertical plane is not controllable. The proposed system aims at achieving a rotation control for a load object shaped like a regular polygon on the vertical plane with respect to the conveyance plate by the one-DoF actuator. First, we introduce the mathematical model and the control input. Second, we report basic behavior of the passive rimless wheel (PRW) with regards to the outer vibration and results of frequency analysis through the numerical simulation. Third, we experimentally verify the results of the numerical simulation. The ARW entrains the walking frequency of the PRW in both the simulations and the experiments, and it indicates controllability of the transition speed for the ARW by the proposed conveyor system.

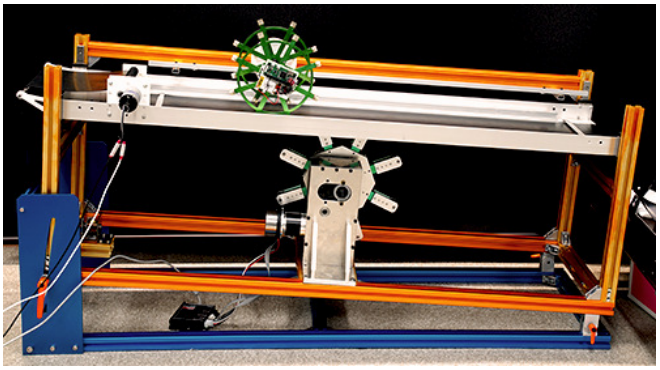

Fig. 1: Prototype experimental system of vibratory conveyor system

II. MATHEMATICAL MODEL

A. Proposed Vibratory Conveyor and PRW

The mathematical model is illustrated in Fig. 2, where the subscript numbers, $i = \{0, 1\}$, respectively indicate a ARW and a PRW as a load object in this paper. Meaning of the symbols are as follows:

m_i [kg]	the masses;
I_i [kg·m^2]	the inertia moments for each mass;
l_i [m]	the length of legs;
α_i [rad]	the half of the step angles;
θ_i [rad]	the angular positions of each stance leg with respect to vertical;
(x_1, z_1) [m]	the tip position of the stance leg for the conveyed RW;
m_p [kg]	the mass of the plate;
$(x_\mathrm{p}, z_\mathrm{p})$ [m]	the position of the plate;

*This research was partially supported by Grant-in-Aid for Scientific Research (C) No. 19K04255, provided by the Japan Society for the Promotion of Science (JSPS).

The authors are with the School of Information Science, Japan Advanced Institute of Science and Technology, Asahidai 1-1, Nomi, Ishikawa 923-1292, Japan {s1810177,s1820026,fasano}@jaist.ac.jp

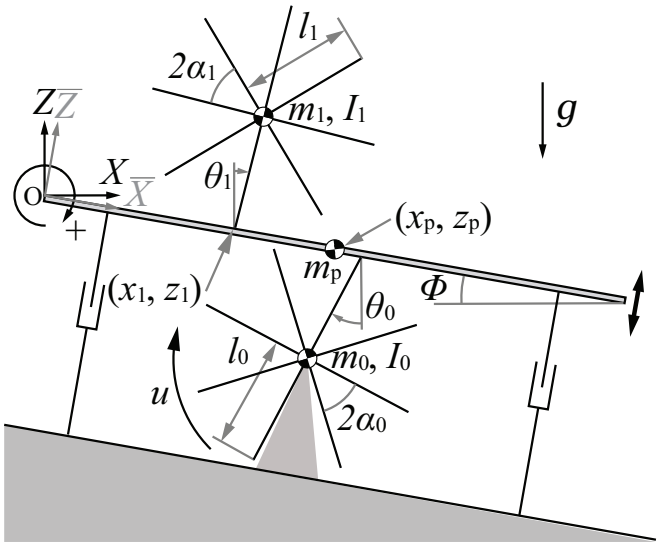

Fig. 2: Mathematical model of proposed vibratory conveyor system

Φ [rad] the table angle with reference to horizon;
u [N·m] the input torque for the ARW.

In this paper, we define a rotation matrix with respect to Φ as

$$\boldsymbol{R}(\Phi) = \begin{bmatrix} C_\Phi & -S_\Phi \\ S_\Phi & C_\Phi \end{bmatrix}. \tag{1}$$

In this paper, S_ξ and C_ξ respectively indicate $\sin(\xi)$ and $\cos(\xi)$, where $\xi \in [-\pi\ \ \pi]$. The rotated coordinates and gravity vector are following.

$$\bar{\boldsymbol{r}}_\eta = \boldsymbol{R}(\Phi)\,\boldsymbol{r}_\eta,\ \bar{\boldsymbol{\theta}} = \boldsymbol{\theta} - \Phi,\ \bar{\boldsymbol{g}} = \boldsymbol{R}(\Phi)\,\boldsymbol{g} \tag{2}$$

Here, the coordinates symbolize $\boldsymbol{r}_\eta = \begin{bmatrix} x_\eta & z_\eta \end{bmatrix}^\mathrm{T}$, $\boldsymbol{\theta} = \begin{bmatrix} \theta_0 & \theta_1 \end{bmatrix}^\mathrm{T}$, $\boldsymbol{g} = \begin{bmatrix} 0 & -g \end{bmatrix}^\mathrm{T}$, $\eta = \{1,\ \mathrm{p}\}$.

B. Equation of Motion

Let $\boldsymbol{q} = \begin{bmatrix} \bar{\theta}_0 & \bar{z}_\mathrm{p} & \bar{x}_1 & \bar{\theta}_1 \end{bmatrix}^\mathrm{T}$ be the generalized coordinate vector, the equation of motion then becomes

$$\boldsymbol{M}\ddot{\boldsymbol{q}} + \boldsymbol{h} = \boldsymbol{S}u + \boldsymbol{J}^\mathrm{T}\boldsymbol{\lambda},\ \boldsymbol{J}\dot{\boldsymbol{q}} = \boldsymbol{0}_{2\times 1}. \tag{3}$$

Here, $\boldsymbol{M} \in \mathbb{R}^{4\times 4}$ is the inertia matrix which is positive definite symmetric; $\boldsymbol{h} \in \mathbb{R}^4$ is the combination vector of central, Coriolis and gravity force; $\boldsymbol{S} = \begin{bmatrix} 1 & 0 & 0 & 0 \end{bmatrix}^\mathrm{T}$ is the control input vector; $\boldsymbol{\lambda} \in \mathbb{R}^2$ is a Lagrange multiplier vector. These details are as follows.

$$\boldsymbol{M} = \begin{bmatrix} I_0 & 0 & 0 & 0 \\ & m_\mathrm{p} & 0 & 0 \\ & & m_1 & -m_1 l_1 S_{\bar{\theta}_1} \\ \mathrm{Sym.} & & & I_1 + l_1^2 m_1 \end{bmatrix}$$

$$\boldsymbol{h} = \begin{bmatrix} 0 \\ g m_\mathrm{p} C_\Phi \\ m_1\left(g C_\Phi - \dot{\bar{\theta}}_1^2 l_1 C_{\bar{\theta}_1}\right) \\ -m_1 g l_1 S_{\bar{\theta}_1 + \Phi} \end{bmatrix}$$

We omitted the half of the detail in the inertia matrix because of the symmetry. The motion should satisfy the following conditions.

- The ARW connects with a base frame by a revolute joint at a cross point of the legs.
- The PRW does not jump during the whole motion.

To mathematically express the previous conditions gives the following holonomic constraint.

$$\boldsymbol{J}\dot{\boldsymbol{q}} = \begin{bmatrix} l_0 S_{\bar{\theta}_0} & 1 & 0 & 0 \\ 0 & 1 & -1 & 0 \end{bmatrix}\dot{\boldsymbol{q}} = \boldsymbol{0}_{2\times 1} \tag{4}$$

The time derivative of Eq. (4) then becomes

$$\boldsymbol{J}\ddot{\boldsymbol{q}} = -\dot{\boldsymbol{J}}\dot{\boldsymbol{q}} = -\begin{bmatrix} l_0\dot{\bar{\theta}}_0 C_{\bar{\theta}_0} & 0 & 0 & 0 \\ 0 & 0 & 0 & 0 \end{bmatrix}\dot{\boldsymbol{q}}, \tag{5}$$

substituting Eq. (5) into Eq. (3) gives

$$\boldsymbol{\lambda} = -\boldsymbol{X}^{-1}\left(\boldsymbol{J}\boldsymbol{M}^{-1}(\boldsymbol{S}u - \boldsymbol{h}) + \dot{\boldsymbol{J}}\dot{\boldsymbol{q}}\right), \tag{6}$$

where $\boldsymbol{X} := \boldsymbol{J}\boldsymbol{M}^{-1}\boldsymbol{J}^\mathrm{T}$.

C. Equation of Collision

We assume the following conditions during the whole motion.

- The collisions between each RW and the plate are completely inelastic.
- These motion does not include a double support phase because the support leg exchanges the swing leg immediately after impact.

Let $\boldsymbol{q}_\mathrm{c} = \begin{bmatrix} \bar{\theta}_0 & \bar{z}_\mathrm{p} & \bar{x}_1 & \bar{z}_1 & \bar{\theta}_1 \end{bmatrix}^\mathrm{T}$ be the generalized coordinate vector for the collision model, the equation of collision then becomes

$$\boldsymbol{M}_\mathrm{c}\dot{\boldsymbol{q}}_{\mathrm{c}i}^{+} = \boldsymbol{M}_\mathrm{c}\dot{\boldsymbol{q}}_\mathrm{c}^{-} + \boldsymbol{J}_{\mathrm{c}i}^\mathrm{T}\boldsymbol{\lambda}_{\mathrm{c}i},\ \boldsymbol{J}_{\mathrm{c}i}\dot{\boldsymbol{q}}_{\mathrm{c}i}^{+} = \boldsymbol{0}_{3\times 1}. \tag{7}$$

Here, the superscriptions '$+$' and '$-$' respectively symbolize immediately after and before impact. The detail of the inertia matrix for collision, $\boldsymbol{M}_\mathrm{c} \in \mathbb{R}^{5\times 5}$, is

$$\boldsymbol{M}_\mathrm{c} = \begin{bmatrix} I_0 & 0 & 0 & 0 & 0 \\ & m_\mathrm{p} & 0 & 0 & 0 \\ & & m_1 & 0 & m_1 l_1 C_{\bar{\theta}_1} \\ & & & m_1 & -m_1 l_1 S_{\bar{\theta}_1} \\ \mathrm{Sym.} & & & & I_1 + l_1^2 m_1 \end{bmatrix}, \tag{8}$$

we omitted the half of the detail in the inertia matrix because it is positive definite symmetry. The collision model contains two cases: collision of the ARW, and the PRW with the plate. Expressing by the subscript numbers, the Jacobian for each case becomes

$$\boldsymbol{J}_{\mathrm{c}0} = \begin{bmatrix} l_0 S_{2\alpha_0 - \bar{\theta}_0} & -1 & 0 & 0 & 0 \\ 0 & 0 & 1 & 0 & 0 \\ 0 & 1 & 0 & -1 & 0 \end{bmatrix}, \tag{9}$$

$$\boldsymbol{J}_{\mathrm{c}1} = \begin{bmatrix} l_0 S_{\theta_0} & 1 & 0 & 0 & 0 \\ 0 & 0 & 1 & 0 & l_1\left(C_{\bar{\theta}_1} - C_{2\alpha_1 - \bar{\theta}_1}\right) \\ 0 & 1 & 0 & -1 & -l_1\left(S_{\bar{\theta}_1} + S_{2\alpha_1 - \bar{\theta}_1}\right) \end{bmatrix}. \tag{10}$$

The momentum dissipation for each case is determined as

$$\boldsymbol{\lambda}_{\mathrm{c}i} = \boldsymbol{M}_\mathrm{c}^{-1}\boldsymbol{J}_{\mathrm{c}i}^\mathrm{T}\boldsymbol{X}_{\mathrm{c}i}^{-1}\boldsymbol{J}_{\mathrm{c}i},\ \boldsymbol{X}_{\mathrm{c}i} := \boldsymbol{J}_{\mathrm{c}i}\boldsymbol{M}_\mathrm{c}^{-1}\boldsymbol{J}_{\mathrm{c}i}^\mathrm{T}. \tag{11}$$

Substituting Eq. (11) into Eq. (7) gives the velocities of each case immediately after impact as follows.

$$\dot{\boldsymbol{q}}_{\mathrm{c}i}^{+} = \left(\boldsymbol{I}_5 - \boldsymbol{M}^{-1}\boldsymbol{J}_{\mathrm{c}i}^\mathrm{T}\boldsymbol{X}_{\mathrm{c}i}^{-1}\boldsymbol{J}_{\mathrm{c}i}\right)\dot{\boldsymbol{q}}_{\mathrm{c}i}^{-} \tag{12}$$

In addition, each stance leg should exchange at the collision timing because of previous assumption, hence the positions for each case are

$$\boldsymbol{q}_{\mathrm{c0}}^{+} = \boldsymbol{q}_{\mathrm{c}}^{-} + \begin{bmatrix} -2\alpha_0 & 0 & 0 & 0 & 0 \end{bmatrix}^{\mathrm{T}},$$
$$\boldsymbol{q}_{\mathrm{c1}}^{+} = \boldsymbol{q}_{\mathrm{c}}^{-} + \begin{bmatrix} 0 & 0 & 0 & 0 & -2\alpha_1 \end{bmatrix}^{\mathrm{T}}. \quad (13)$$

D. Control Input

We determine the control output as $y = \boldsymbol{S}^{\mathrm{T}}\boldsymbol{q} = \theta_0$, the second order time derivative then becomes

$$\ddot{y} = \boldsymbol{S}^{\mathrm{T}}\ddot{\boldsymbol{q}} = \boldsymbol{S}^{\mathrm{T}}\boldsymbol{M}^{-1}\left(\boldsymbol{S}u - \boldsymbol{h} + \boldsymbol{J}^{\mathrm{T}}\boldsymbol{\lambda}\right). \quad (14)$$

To define $y_{\mathrm{d}}(t) \in \mathbb{R}$ as a desired time trajectory, the control input to achieve $y \to y_{\mathrm{d}}(t)$ can be obtained as

$$u = A^{-1}(v + B), \ v = \ddot{y}_{\mathrm{d}}(t) + K_{\mathrm{D}}\dot{y}_{\mathrm{e}} + K_{\mathrm{P}}y_{\mathrm{e}}, \quad (15)$$
$$A := \boldsymbol{S}^{\mathrm{T}}\boldsymbol{M}^{-1}\boldsymbol{Y}\boldsymbol{S}, \ B := \boldsymbol{S}^{\mathrm{T}}\boldsymbol{M}^{-1}\left(\boldsymbol{Y}\boldsymbol{h} + \boldsymbol{J}^{\mathrm{T}}\boldsymbol{X}^{-1}\dot{\boldsymbol{J}}\dot{\boldsymbol{q}}\right),$$
$$\boldsymbol{Y} := \boldsymbol{I}_4 - \boldsymbol{J}^{\mathrm{T}}\boldsymbol{X}^{-1}\boldsymbol{J}\boldsymbol{M}^{-1}, \ y_{\mathrm{e}} := y_{\mathrm{d}}(t) - y,$$

where K_{P} and K_{D} are PD gains. In this paper, we consider the desired time trajectory as

$$y_{\mathrm{d}}(t) = \omega T - \alpha_0, \ T := t - t_{\mathrm{c0}}[n] \quad (n \in \mathbb{Z}_0^{+}), \quad (16)$$

where $t_{\mathrm{c0}}[n]$ is the timing at n-th collision for the ARW and $t_{\mathrm{c0}}[0] = 0$ [s].

III. NUMERICAL SIMULATION

A. System Parameter and Initial State

The system parameters are listed in Table I, and the initial states of the simulation are

$$\boldsymbol{q}(0) = \begin{bmatrix} -\alpha_0 & l_0 C_{y_{\mathrm{d}}(0)} & l_0 C_{y_{\mathrm{d}}(0)} & -\alpha_1 \end{bmatrix}^{\mathrm{T}}$$
$$= \begin{bmatrix} -\alpha_0 & l_0 C_{\alpha_0} & l_0 C_{\alpha_0} & -\alpha_1 \end{bmatrix}^{\mathrm{T}},$$
$$\dot{\boldsymbol{q}}(0) = \begin{bmatrix} \omega & -\omega l_0 S_{\alpha_0} & -l_0 \omega S_{\alpha_0} & 3 \end{bmatrix}^{\mathrm{T}}. \quad (17)$$

The following simulations use these parameters when we do not specify a different value for these parameters. The PRW motion does not converge for a while due to the initial angular velocity, thereby we show the results after 150-th collision of the PRW to clarify the vibration effect. In this paper, the frequency of the vibration for the conveyance plate and the walking frequency for the PRW respectively symbolize f_{p} and f_{w} [Hz], these definitions are

$$f_{\mathrm{p}} = \frac{\omega}{2\alpha_1}, \ f_{\mathrm{w}} = \frac{1}{t_{\mathrm{c1}}[n] - t_{\mathrm{c1}}[n-1]} \quad (n \in \mathbb{Z}^{+}). \quad (18)$$

Here, $t_{\mathrm{c1}}[n]$ is the timing at n-th collision for the PRW and $t_{\mathrm{c1}}[0] = 0$ [s].

TABLE I: System parameters

m_0	1.5	kg
l_0	0.15	m
I_0	0.15	kg·m^2
α_0	π/8	rad
m_{p}	6.0	kg
g	9.81	m/s^2
Φ	π/60	rad

m_1	0.6	kg
l_1	0.1	m
I_1	0.06	kg·m^2
α_1	π/8	rad
K_{D}	100	s^{-1}
K_{P}	2500	s^{-2}

B. Representative Behavior

Fig. 3 shows results of a representative behavior where $f_{\mathrm{p}} = \{2.0,\ 4.5\}$ [Hz]. Here, Fig. 3 (a) is the angular velocity data for the PRW, and Fig. 3 (b) is the phase-space diagram of the passiveRW for 6 collisions. Fig. 4 illustrates the stick diagrams for Fig. 3, where Fig. 3 (a) and Fig. 3 (b) are respectively denote when $f_{\mathrm{p}} = 2.0$ [Hz] and $f_{\mathrm{p}} = 4.5$ [Hz]. The phase-space diagram and the stick diagrams indicate the time transition by the lightness, which gets high value at earlier time.

The angular velocity of the PRW frequently shows rapid changing, because of the collision timing of the ARW. The collision of the ARW gives a torque to the PRW, the torque can be specified as

$$\tau_{\mathrm{c1}} = F_{\mathrm{c}} l_1 S_{\bar{\theta}_1}. \quad (19)$$

Here, F_{c} is a force which occurs during the collision of the ARW. Therefore, the collision of the ARW reduces the angular momentum of the PRW when $\bar{\theta}_1 < 0$, whereas it enlarges the angular momentum when $\bar{\theta}_1 > 0$. On the frequency, the average frequency of f_{w} becomes $\{4.45,\ 4.56\}$ [Hz] when $f_{\mathrm{p}} = \{2.0,\ 4.5\}$ [Hz], respectively. The difference on the average frequency of f_{w} indicates controllability on the walking speed of the PRW.

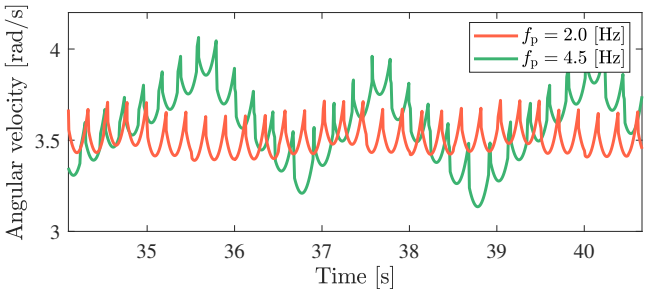

(a) Time transition of angular velocity for PRW

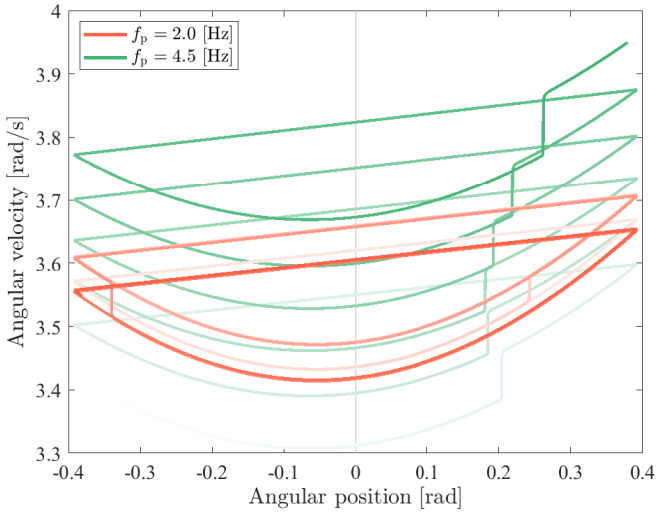

(b) Phase-space diagram for PRW

Fig. 3: Representative behavior

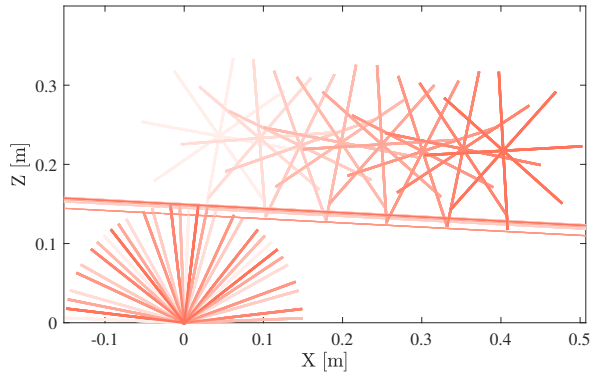

(a) $f_{\mathrm{p}} = 2.0$ [Hz]

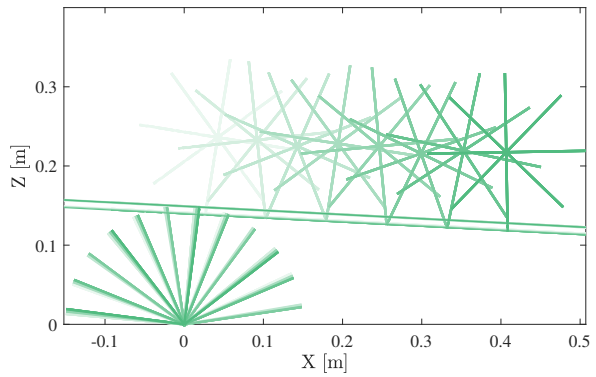

(b) $f_{\mathrm{p}} = 4.5$ [Hz]

Fig. 4: Stick diagrams for the representative behavior

C. Analysis for Frequency Entrainment

In the previous section, the frequency of the ARW effects the walking frequency of the PRW. To investigate the relationship between f_{p} and f_{w}, we numerically analyze the transition tendency of f_{w} with respect to f_{p}. The analysis procedure is as follows:

P1) Set $\omega = 0$ [rad/s].
P2) Set the initial states as Eq. (17).
P3) Simulate between $n \in [0\ 180]$ [step].
P4) Increase ω by 0.1 [rad/s].
P5) Repeat from P2 when $\omega \leq 10.0$ [rad/s].

The analysis result using the system parameters listed in Table I is shown in Fig. 5. In the analysis, the gray line denotes $f_{\mathrm{w}} = f_{\mathrm{p}}$ and the gray dashed-line intends $f_{\mathrm{w}} = 2f_{\mathrm{p}}$. f_{w} almost takes the frequency of passive dynamic walking which is the value of the frequency for the PRW when $f_{\mathrm{p}} = 0$ [Hz] in the low frequency band. On the other hand, f_{w} becomes divergence as the ARW frequency increases in high frequency band. The yellow area means frequency entrainment, $f_{\mathrm{w}} = f_{\mathrm{p}}$ appears approximately $f_{\mathrm{p}} \in [4\ 5]$ [Hz], and $f_{\mathrm{w}} = 2f_{\mathrm{p}}$ also appears approximately $f_{\mathrm{p}} \in [8\ 10]$ [Hz]. $f_{\mathrm{w}} = f_{\mathrm{p}}$ entrainment range is useful to control the frequency of the PRW, however the motion of the PRW is not steady in $f_{\mathrm{w}} = 2f_{\mathrm{p}}$ entrainment range.

It was already clarified that the amplitude enlarges the entrainment range in [8]. Therefore, taking a long leg expands the entrainment range, because the leg length of the ARW

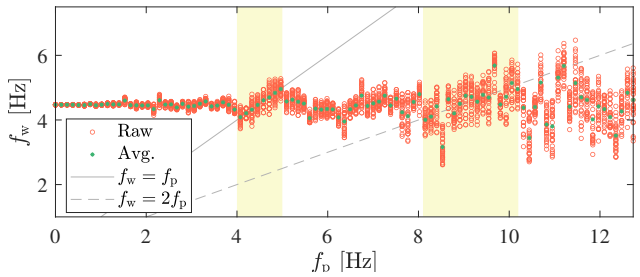

Fig. 5: f_{w} versus f_{p}

decides the amplitude of the plate vibration. The leg length effects the entrainment range, meanwhile it contains risks as follows: the ground reaction force becomes negative; the dispersion on the frequency of the PRW becomes high. We analyze the transition tendency of f_{w} for two values of l_0 to ascertain them, the results are shown in Fig. 6. Fig. 6 (a) and Fig. 6 (b) respectively show the analysis results for $l_0 = 0.1$ [m] and $l_0 = 0.2$ [m]. The long leg enlarges the $f_{\mathrm{w}} = f_{\mathrm{p}}$ entrainment range, whereas $f_{\mathrm{w}} = 2f_{\mathrm{p}}$ entrainment range becomes unclear due to the dispersion. In addition, the dispersion also becomes high in the $f_{\mathrm{w}} = f_{\mathrm{p}}$ entrainment range.

The leg length of the PRW changes the entrainment range, hence identifying a defective item becomes possible by setting the frequency of the plate carefully. The analysis results for two cases of l_1 are shown in Fig. 7, where Fig. 7 (a) and Fig. 7 (b) respectively show the analysis results for $l_1 = 0.08$ [m] and $l_1 = 0.12$ [m]. Each entrainment range shifts to the low frequency direction when the leg of the PRW takes long length, thereby the conveyor system identifies fatal defective items on the shape by setting the frequency studiously.

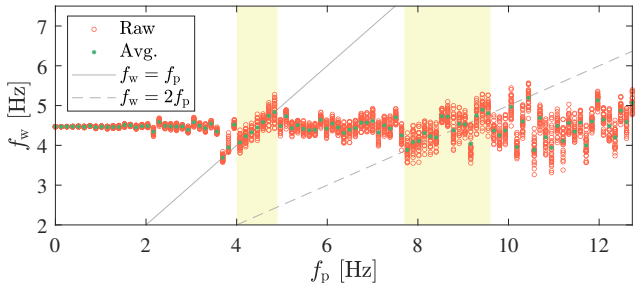

(a) $l_0 = 0.1$ [m]

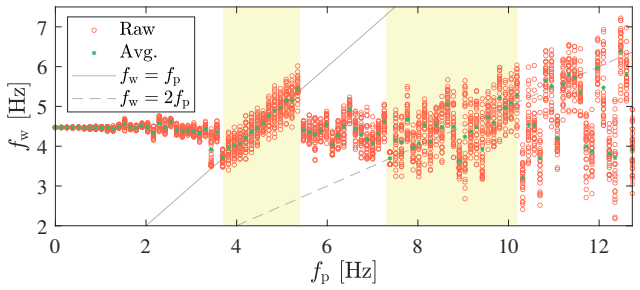

(b) $l_0 = 0.2$ [m]

Fig. 6: f_{w} versus f_{p} for two values of l_0

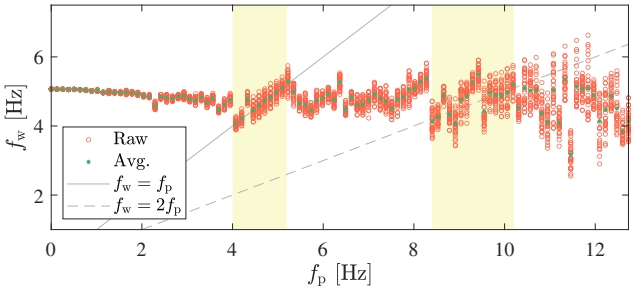

(a) $l_1 = 0.08$ [m]

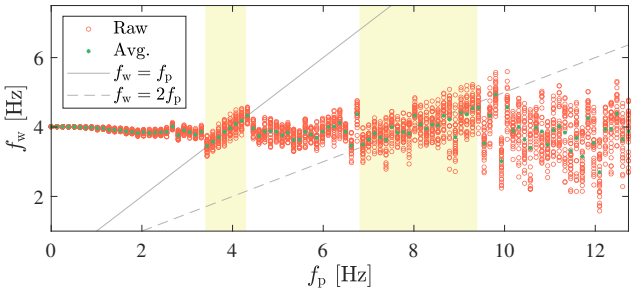

(b) $l_1 = 0.12$ [m]

Fig. 7: f_w versus f_p for two values of l_1

IV. EXPERIMENTAL VERIFICATION

A. Experimental System and Environment

The experimental machine is shown in Fig. 1, where the ARW is placed under the conveyance plate and a rubber belt on the conveyance plate substitutes a treadmill by winding the rubber belt. The ARW connects with a electronically commutated (EC) motor, which is controlled by digital positioning controller, at the rotation center. Fig. 8 gives the overview of the PRW, where the electronic circuit acquires the angular velocity and the acceleration data. These component parts are mainly listed in Table II. We estimate the angular position of the PRW by using Kalman filter.

B. Verification

Fig. 9 shows the contours which are extracted in 3 [Hz] where $f_p = 2.05$ [Hz], the gradation indicates the time

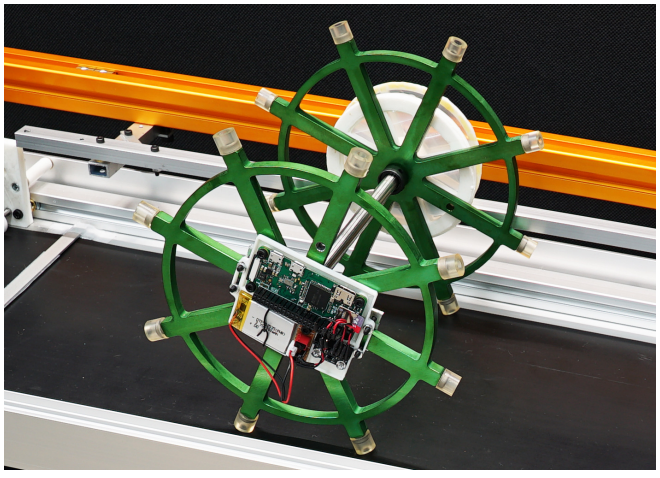

Fig. 8: Overview of PRW

TABLE II: Component parts

EC motor	EC 90 flat
Digital position controller	EPOS2 P 24/5
Single board computer	Raspberry pi zero
Sensor	MPU6050

transition. Fig. 10 shows the time transition on the angular velocity of the PRW, where Fig. 10 (a) and 10 (b) are the results for $f_p = 2.05$ [Hz] and $f_p = 3.00$ [Hz], respectively. The red line is the raw data, and the green line is the filtering data which gives a moving average. The vibration of the conveyance plate significantly effects the angular velocity when $f_p = 3.00$ [Hz]. The phase-space diagram for the PRW is drawn as Fig. 11, the angular position includes errors of the estimation. The errors mainly appear in the difference of the estimating step angle and occur by the collision of the ARW and the PRW.

Fig. 12 shows the frequency analysis results to compara-

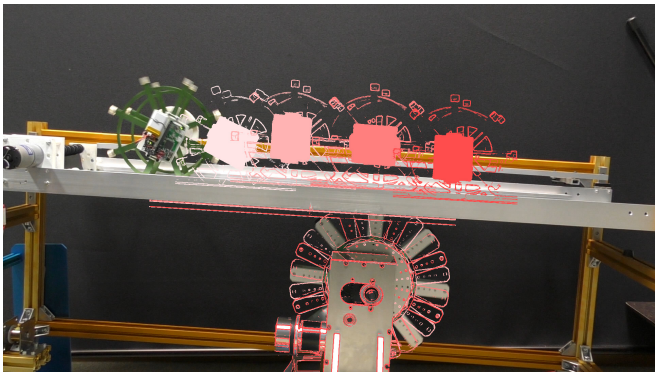

Fig. 9: Contours by 3 [Hz] where $f_p = 2.05[Hz]$

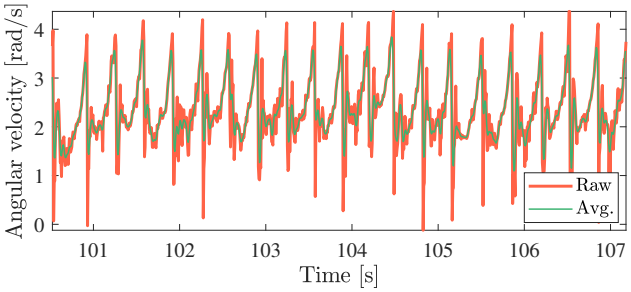

(a) $f_p = 2.05$ [Hz]

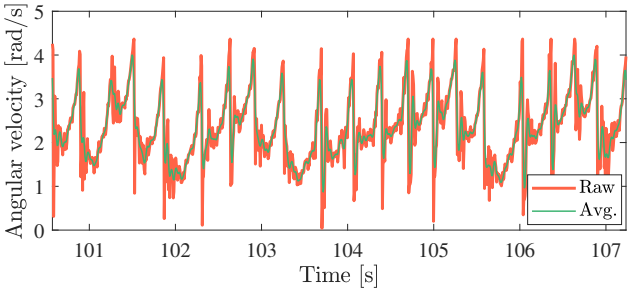

(b) $f_p = 3.00$ [Hz]

Fig. 10: Time transition of angular velocity for PRW

tively investigate the numerical simulation and experiment, Fig. 12 (a) is the simulation result by estimating the inertia moment of the PRW on the experimental system, whose value becomes $I_1 = 0.004$ [kg·m^2], and Fig. 12 (b) is the experimental result. The entrainment range appears approximately between $f_\mathrm{p} \in [2.6\ 3]$ [Hz] in the experiment, where 3 [Hz] is the limitation of the prototype experimental system. Therefore, the entrainment range can be extended to more high frequency area as shown in Fig. 12 12a. The experimental results are similar to the simulation results in the entrainment range as well as the dispersion.

V. CONCLUSION AND FUTURE WORK

In this paper, we proposed the vibratory conveyor system based on the frequency entrainment of the limit cycle walker.

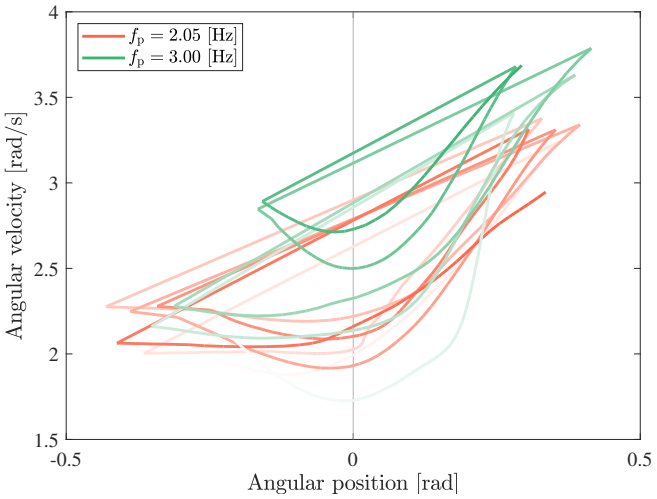

Fig. 11: Phase-space diagram for PRW

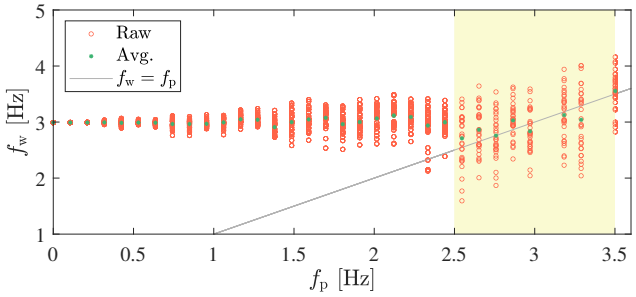

(a) Simulation

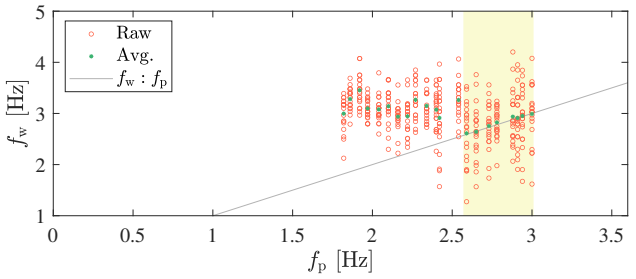

(b) Experiment

Fig. 12: Comparison of f_w versus f_p

First, we introduced the mathematical model and the control to investigate the generating motion as well as the frequency entrainment range numerically. Second, we showed the representative motion of the vibratory conveyor system. The plate vibration induces the fluctuation on the angular velocity of the PRW. Third, we investigated the relationship between the frequency on walking of the PRW and the vibration of the conveyance plate. The vibration of the conveyance plate significantly effects the walking of the PRW, the walking frequency is entrained to the vibration frequency of the conveyance plate. Extending the leg length of the ARW enlarged the entrainment range, whereas it disperses the walking frequency of the PRW. We observed that the leg length of the PRW shifts the frequency entrainment range, the shift of the entrainment range indicates a possibility to identify fatal defective items on the shape difference. Fourth, we verify the simulation results by using the prototype experimental system. The experimental results showed similar tendency with the simulation results in the entrainment range as well as the dispersion.

The dispersion on the walking frequency of the PRW is still large, the motion of the PRW does not converge a steady motion enough. Therefore, devising a control input to converge the walking frequency based on the dynamics of the limit cycle walker is the most important work in the future. Developing an experimental system which can verify in higher frequency range is also left as a future work.

REFERENCES

[1] M. Reis, "Vibration based under-actuated bounding mechanism", *Int. J of Intelligent and Robotic Systems*, Vol. 82, pp. 455–466, 2016.

[2] P. Liu, H. Yu and S. Cang, "On the dynamics of a vibro-driven capsule system", *Int. J. of Archive of Applied Mechanics*, pp. 2199-–2219, 2018.

[3] F. Asano, T. Seino et al. "A novel locomotion robot that slides and rotates on slippery downhill," *Proc. of Int. Conf. on Advanced Intelligent Mechatronics*, pp. 425–430, 2016.

[4] M. Nishihara and F. Asano, "Experimental verification of underactuated sliding locomotion robot with quick return linkage," *Proc. of Int. Conf. on Robotics and Biomimetics*, pp. 1359–1364, 2018.

[5] Y. Cal, S. Suzuki and Y. Hoshino, "Gait stabilization of a quasi-passive walker based on energy balance by utilizing a mechanical oscillator," *Proc. of Int. Conf. on Asian Control Conference*, pp. 1–6, 2015.

[6] Y. Hanazawa, "Development of rimless wheel with controlled wobbling mass," *Proc. of Int. Conf. on Intelligent Robots and Systems*, pp. 4333–4339, 2018.

[7] F. Asano and I. Tokuda, "Indirectly controlled limit cycle walking of combined rimless wheel based on entrainment to active wobbling motion," *Int. J. of Multibody System Dynamics*, Vol. 34, Issue. 2, pp. 191–210, 2015.

[8] L. Li, I. Tokuda and F. Asano, "Optimal input waveform for an indirectly controlled limit cycle walker," *Proc. of Int. Conf. on Intelligent Robots and Systems*, pp. 7454–7459, 2018.

[9] H. Chen, S. Jiang et al., "A simulation study on conveying characteristics of particles on a vibrating plate with zigzag morphology," *Proc. of Int. Conf. on Information and Automation*, pp. 468–473, 2016.

[10] P. U. Frei, "An intelligent vibratory conveyor for the individual object transprtation in two dimensions," *Proc. of Int. Conf. on Intelligent Robots and Systems*, pp. 1832–1837, 2002.

[11] M. Higashimori, R. Sakashita and A. Shibata, "Single-actuator-based three-DoF planar manipulation via a viscoelastic and nonparallel hybrid joint mechanism," *Int. J. of Transactions on Robotics*, Vol. 35, No.3, pp. 602–617, 2019.